Journal of Sound and Vibration (1997) **202**(5), 717–731

HARMONIC BALANCE AND CONTINUATION TECHNIQUES IN THE DYNAMIC ANALYSIS OF DUFFING'S EQUATION

K. B. Blair

Moldyn, Inc., 955 *Massachusetts Avenue*, *Cambridge*, *MA* 02139, *U.S.A.*

C. M. Krousgrill

School of Mechanical Engineering, *Purdue University*, *West Lafayette*, *IN* 47907, *U.S.A.*

AND

T. N. Farris

School of Aeronautics and Astronautics, *Purdue University*, *West Lafayette IN* 47907, *U.S.A.*

(*Received* 29 *August* 1994, *and in final form* 8 *November* 1996)

Duffing's equation with a negative linear stiffness is investigated. A harmonic balance technique coupled with a continuation scheme is utilized to trace the system response to changes in the magnitude of the applied harmonic forcing. With the aid of Floquet theory, the stability of the resulting solutions is ascertained. The use of the analysis technique described herein allows for the identification of previously undetected strange attractors that coexist with the stable period one solutions. These results explain the discrepancies between the observed and theoretically predicted levels of applied loading required for chaotic motion.

1. INTRODUCTION

The dynamic response of Duffing's equation to harmonic forcing has been studied in a large number of papers, in an effort to understand the parameters surrounding the onset of chaotic response. Holmes [1] studied Duffing's equation with a negative linear stiffness as a single-mode model of a buckled beam undergoing forced lateral vibrations. For normalized parameters, the equation is expressed as

$$\ddot{x} + \gamma\dot{x} - \tfrac{1}{2}x(1 - x^2) = F \sin \omega t. \tag{1}$$

For the case of $F = 0$, the equation has three static equilibrium positions, $x = \pm 1$ and $x = 0$. It can be shown that the non-zero equilibrium positions are dynamically stable and the center, $x = 0$, equilibrium position is unstable with respect to infinitesimal disturbances [1]. Linearizing the equation of motion about the stable, static equilibrium states of $x = \pm 1$ results in a second order system with natural frequency $\omega_0 = 1$.

Dynamically, equation (1) is globally stable, in that after a sufficient passage of time, all solutions enter and remain within a bounded region of the x–$\dot{x}$ phase space [2]. Thus, the system has at least one attractor. The character of the dynamic response to harmonic excitation is dependent on the magnitude of the applied load. For small levels of excitation,

0022–460X/97/200717 + 15 $25.00/0/sv960853

there are attracting periodic orbits encircling the stable equilibrium positions. For other system parameters remaining constant, the size of the periodic orbits are dependent on the magnitude of the applied load. Additionally, a saddle-type periodic orbit exists that passes through the unstable equilibrium position. For large values of the applied load, the motion encircles all of the equilibrium positions. In between these values of applied loading, there are regions of period-doubling behavior, the period of the response being half that of the excitation, and chaotic motion occurs. Investigators have used the term "strange attractor" to denote these types of bounded, chaotic non-periodic solutions of deterministic, non-linear differential equations.

The birth of the strange attractor is theoretically connected to the intersection of the stable and unstable orbits in the phase space. After the technique of Mel'nikov [3], Holmes [1] derived a critical force level, at which the intersection of the stable and unstable solution manifolds is expected to occur. For equation (1), this can be expressed as

$$F_M = \frac{\gamma\sqrt{2}}{3\pi\omega}\cosh\left(\frac{\pi\omega}{\sqrt{2}}\right). \tag{2}$$

This critical force would correspond to a necessary condition for chaotic motion, and will be subsequently referred to as the Mel'nikov force value.

Since the presentation of that equation, researchers have attempted to verify its accuracy, determine the physical events surrounding the initiation of chaotic behavior, and provide insight as to the character of chaotic behavior. Moon and Holmes [2] used a steel cantilever beam buckled by the influence of magnets at the free end to experimentally verify the behavior of Duffing's equation. For many combinations of the values of the forcing amplitude and frequency, a boundary was experimentally determined at which chaotic motion was first observed. Additionally, certain values of the forcing amplitude and frequency resulted in transient chaotic motion, defined as chaotic motion that eventually settled to periodic motion. It was found that the predicted chaos boundary from equation (2) was a good indicator of transient chaotic motion. Sustained chaotic motion occurred for significantly higher values of the forcing amplitude than that predicted by equation (2).

Dowell and Pezeshki [4] performed a detailed study of Duffing's equation. By numerically integrating equation (1) starting from many sets of initial conditions, a zero-region boundary was defined in the x–$\dot{x}$ phase space. This region corresponded to the region of the phase space in which the motion from a given set of initial conditions never crossed $x = 0$. For the case of forced response, numerical integration was used to plot the trajectories for several values of the magnitude of the applied loading. For the values of $\gamma = 0{\cdot}168$ and $\omega = 1{\cdot}0$, two-period motion was found to occur at $F = F_P = 0{\cdot}177$, and was assumed to arise from a bifurcation in the solution. This value of forcing amplitude will be termed the nominal period-doubling force. Further period-doubling behavior was observed, and chaotic motion was first observed for $F = F_C = 0{\cdot}205$, subsequently referred to as the nominal chaos force, a value significantly higher than that predicted by equation (2), $F_M = 0{\cdot}1176$ [5]. It was observed that at force levels slightly below the first observed occurrence of chaos, the above-described zero region boundary was crossed by the solution trajectories. As a result, it was hypothesized that the crossing of the zero-region boundary corresponded to a minimum value of forcing magnitude to cause chaos. Additionally, the first observance of chaos for various values of the applied forcing magnitude and frequency were found, again using numerical integration. The results suggest that regions of chaotic response lie in fragmented regions of the force–frequency plane. Indeed, this has been shown to be true by Moon [6].

Pezeshki and Dowell [5] furthered their study by developing basin-boundary maps for equation (1). These maps were developed for a given set of system parameters by numerically integrating the equation of motion until the transients for a given set of initial conditions dissipates. By observing which static equilibrium position the resulting steady state motion encircles, a domain of attraction is defined for each of the stable static equilibrium positions. The boundary between the domain of attraction is termed the basin boundary. Below the Mel'nikov force value from equation (2), $F_M = 0{\cdot}1176$, it was found that the basin boundaries are smooth. For force values above the Mel'nikov value, the map becomes more complex, indicating fractal behavior. This signifies a decrease in the ability to predict the final state of the system given the initial conditions and system parameters. As the magnitude of the applied load was increased to the level of chaos observed in their previous work, $F_C = 0{\cdot}205$, the basin boundary map becomes more diffuse, implying that the final state of the system is unknowable for any set of initial conditions. Even though time traces of this behavior appear to have no order, phase portraits of Poincaré maps show a complicated but repeated structure [7].

Additionally, transient time maps [5] have been constructed for equation (1). These maps record the number of periods of the applied forcing required for the transients to decay for a given set of initial conditions. Behavior similar to that described above was observed in the neighborhood of the Mel'nikov force value. Additionally, for $F = F_0 = 0{\cdot}13$, subsequently termed the observable chaos boundary, a certain percentage of the initial conditions never converged to a steady state response while others converged to period one responses. This suggests that a chaotic attractor exists for this force level. Consequently, initial condition maps, corresponding to recording the initial conditions that result in unconverged solutions, were also plotted for the same ranges of forcing. The first occurrence of non-converging solutions was found at a level slightly above the Mel'nikov force level, $F_M = 0{\cdot}1176$. The percentage of unconverged solutions rapidly increased after the forcing amplitude reached the nominal period-doubling boundary, $F_P = 0{\cdot}177$, until the nominal chaos boundary was reached, $F_C = 0{\cdot}205$. At this load value, all of the initial conditions result in unconverged solutions.

As another explanation for the conditions required for observing chaotic response in equation (1), Dowell and Pezeshki [8] found that the stable limit cycle about $x = 1$ and the unstable limit cycle about $x = 0$ intersect at an applied load very close to the nominal chaos force level observed using numerical integration, $F_C = 0{\cdot}205$. Thus, it is stated that the intersection of the stable and unstable limit cycles is a necessary and sufficient condition for the occurrence of steady state chaos.

In summary, for a forcing frequency of $\omega = 1{\cdot}0$, the Mel'nikov force value, which predicts the crossing of the stable and unstable manifold solutions, is $F_M = 0{\cdot}1176$. The lowest observed force amplitude value for chaotic motion is $F_O = 0{\cdot}13$. However, chaotic motion occurred only for select sets of initial conditions. The nominal period-doubling force is $F_P = 0{\cdot}177$, and the nominal chaos force is $F_C = 0{\cdot}205$, each of which correspond to the only observable response for the given force value for any sets of initial conditions. The discrepancy in the above values points to the existence of more than one type of attractor for a given value of forcing, especially for values of the applied loading in the neighborhood of the Mel'nikov force value. Leung and Fung [9], utilizing a type of harmonic balance method, have demonstrated that varying the frequency of the applied load results in turning points in the amplitude–frequency response curves, with multiple steady state periodic solutions. The results presented above point to the fact that this would also be true for the case of a fixed frequency and variable force amplitude. Additionally, the construction of a bifurcation diagram that traces the response variation as a function of the applied loading can provide insight into the characteristics of the various solution

trajectories. The location of the solution bifurcations and subsequent new solution paths can be found by analyzing the stability of the solution path. The resulting portrait of periodic solutions for a range of loading should help explain the above discrepancies in the theoretically predicted and the experimentally and numerically observed chaotic behavior.

2. ANALYSIS TECHNIQUE

In order to determine both stable and unstable periodic solutions to Duffing's equation, the harmonic balance method is employed. The harmonic balance technique results in the non-linear differential equation of motion being solved using a set of non-linear algebraic equations. The application of the technique begins by writing the equation of motion (1) as

$$\ddot{x} = f(\dot{x}, x, t), \tag{3}$$

where, for Duffing's equation

$$f(\dot{x}, x, t) = F \sin \omega t - (\gamma \dot{x} - \tfrac{1}{2}x(1 - x^2)). \tag{4}$$

Since the equation of motion contains harmonic forcing, it is appropriate to investigate periodic, steady state solutions. Thus, the solution of equation (3) can be written in the form of an mT periodic solution as

$$x_{mT}(t) = C_0 + \sum_{j=1}^{N} C_{j/m} \cos\left(\mathrm{j}\,\frac{2\pi}{mT}\,t + \psi_{j/m}\right), \tag{5}$$

with its time derivatives expressed as

$$\dot{x}_{mT}(t) = \sum_{j=1}^{N} -\mathrm{j}\,\frac{2\pi}{mT}\,C_{j/m} \sin\left(\mathrm{j}\,\frac{2\pi}{mT}\,t + \psi_{j/m}\right), \tag{6}$$

and

$$\ddot{x}_{mT}(t) = \sum_{j=1}^{N} -\left(\mathrm{j}\,\frac{2\pi}{mT}\right)^2 C_{j/m} \cos\left(\mathrm{j}\,\frac{2\pi}{mT}\,t + \psi_{j/m}\right). \tag{7}$$

Here, the fundamental period is $T = 2\pi/\omega$, where ω is the frequency of the applied harmonic forcing, and m is an integer corresponding to the ratio of the period of the external forcing to be period of the response. This representation allows periodic solutions other than those of the fundamental period to be found. $C_{j/m}$ and $\psi_{j/m}$ are unknown Fourier coefficients and phase angles that satisfy the equation of motion (3).

Since all terms on the right side of equation (4) are periodic, $f(\dot{x}, x, t)$ can also be expressed as a Fourier series. Thus,

$$f_{mT}(t) = F_0 + \sum_{j=1}^{N} F_{j/m} \cos\left(\mathrm{j}\,\frac{2\pi}{mT}\,t + \phi_{j/m}\right). \tag{8}$$

Substitution of equations (7) and (8) into the equation of motion (3) and balancing the coefficients of each of the harmonic terms produces the desired set of non-linear algebraic equations:

$$F_0 = 0, \qquad F_{j/m} \cos \phi_{j/m} = -\left(\mathrm{j}\frac{2\pi}{mT}\right)^2 C_{j/m} \cos \psi_{j/m},$$

$$F_{j/m} \sin \phi_{j/m} = -\left(\mathrm{j}\frac{2\pi}{mT}\right)^2 C_{j/m} \sin \psi_{j/m}, \tag{9}$$

with the Fourier coefficients and phase angles, $C_{j/m}$ and $\psi_{j/m}$, of the periodic response as the unknowns. Note that $F_{j/m}$ and $\phi_{j/m}$ are functions of $C_{j/m}$ and $\psi_{j/m}$ through the relationships shown in equations (5)–(7). Equations (9) can be solved with the aid of a non-linear algebraic equation solver. Unlike numerical integration, the method allows for convergence to unstable solutions.

The solution to equations (9) proceeds as follows. First, the system parameters under consideration are selected. Next, an initial guess for the Fourier coefficients and phase angles $C_{j/m}$ and $\psi_{j/m}$ is required. For system parameters resulting in a weakly non-linear, stable response, these can be easily obtained by numerically integrating equation (3) until the transients have decayed, and taking a Fast Fourier Transform (FFT) over one period of the response to determine $C_{j/m}$ and $\psi_{j/m}$. It is worth noting that systems exhibiting strong non-linearities often have a nearly linear response under conditions of low excitation levels. Such a case can be used for a starting solution, and the applied loading can be increased as subsequent solutions are found.

By utilizing a non-linear equation solver, the solution proceeds. Using the guesses of $C_{j/m}$ and $\psi_{j/m}$, a time history of $f(\dot{x}, x, t)$ can be easily generated. By selecting a point in time and determining $x(t)$ and $\dot{x}(t)$ from equations (6) and (7), $f(\dot{x}, x, t)$ can be calculated using equation (4) for a given point in time. This can be repeated for an entire period of the applied harmonic load. An FFT algorithm can be used to generate the Fourier coefficients and phase angles, $F_{j/m}$ and $\phi_{j/m}$, from the time history of $f(\dot{x}, x, t)$. Equations (9) can be checked for equivalence, and adjustments to the values of $C_{j/m}$ and $\psi_{j/m}$ can be made. A new time history of $f(\dot{x}, x, t)$ is determined, resulting in new values for $F_{j/m}$ and $\phi_{j/m}$. Equations (9) are checked for equivalence, and the process is repeated until the system converges. Since it is desired to study the effect of the magnitude of the applied load on the system response, this value is systematically varied for subsequent solutions. The previous solution can be used as an initial guess for the subsequent iteration.

As stated above, the results of this parametric variation is expected to yield turning points in the relationship between the magnitude of the applied load and the response amplitude. Using the value of the magnitude of the applied load for an incremental parameter, ΔF, is therefore not feasible. The path shown in Figure 1 represents a solution branch for the equation of motion. The points k and $k-1$ represent solution points determined from the harmonic balance technique. As shown in Figure 1, at a turning point in the solution, the harmonic balance technique would try to find a solution in the neighborhood of point p, where none exists. Thus, a new set of initial guesses for $C_{j/m}$ and $\psi_{j/m}$ would be required that would allow for moving along the upper portion of the branch. Here, using numerical integration may not be of assistance, as the close proximity of the upper and lower sections of the solution branch would make it difficult to find the correct set of initial conditions to converge to a given section of the branch. Additionally, as will be shown later, this type of turning point corresponds to a loss of stability along the solution path. When using a numerical integration technique that is unconditionally stable,

there is no hope of finding a set of initial conditions that would converge to the unstable branch. Consequently, a continuation scheme [10] can be utilized to trace the solution trajectories. Instead of proceeding along the solution path using one of the physical parameters of the system, the arc length of the solution path is used as the control parameter.

Adding the arc length along the solution path as the control parameter allows for the applied load F to be treated as one of the unknown variables, assuming any value required to satisfy the system of equations. Since another unknown is introduced into the system of equations, a relationship between the control parameter of arc length and the unknowns, $C_{j/m}$ and $\psi_{j/m}$, and F is required. Defining incremental arc length, Δs, as the control parameter, the additional equation is written as

$$\Delta s^2 = (F - F^k)^2 + \sum_{i=1}^{2N+1} (\beta_i - \beta_i^k)^2, \tag{10}$$

where the values with the superscript k refer to the last known solution and the values with no superscript refer to the latest available estimate of the solution. Here, F is the magnitude of the applied load, and the β_i are the elements of the vector $\vec{\beta}$ of length $2N + 1$ that contains the Fourier coefficients and phase angles of the solution:

$$\vec{\beta} = [C_0, C_2, C_3, \ldots, C_N, \psi_1, \psi_2, \psi_3, \ldots, \psi_N]^{\mathrm{T}}. \tag{11}$$

Note that the applied load, F, is now an unknown.

The solution strategy can be implemented by employing a predictor–corrector technique. Two sets of Fourier coefficients and phase angles representing solutions to the equation of motion (3) for two values of the applied load can be found by the harmonic balance technique described above. These are used to calculate a predictor value, point p in Figure 1. For the case of the linear predictor, the predictor value can be written in terms of the two known solutions as

$$\beta_i^p = 2\beta_i^k - \beta_i^{k-1} \qquad \text{and} \qquad F_i^p = 2F_i^k - F_i^{k-1}, \tag{12}$$

where the superscripts k and $k - 1$ refer to values corresponding to the two previously determined solutions, the superscript p refers to the value of the predictor, and the subscript i refers to the Fourier coefficient. Using the predictor values as an initial guess to the solution, the non-linear equation solution routine outlined above is used to

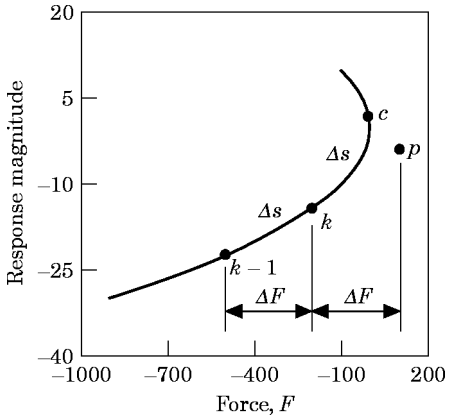

Figure 1. A typical solution trajectory.

simultaneously solve equations (9) and (10) for the unknown load, F, and the Fourier coefficients and phase angles of the response $\vec{\beta}$. The newly found values of F and $\vec{\beta}$ are saved to be used in equation (12) for future predictor steps. The process is repeated until the desired range of parameters is investigated. Thus, it is seen that utilizing the incremental arc length as a control parameter allows the load, F, and the Fourier coefficients and phase angles, $\vec{\beta}$, to assume any values necessary to satisfy the equilibrium relations. This allows solution branches and turning points of both stable and unstable solutions to be systematically traced.

In certain cases, the solution may approach limit points in the solution space. In this case, scaling the parameters can aid the convergence of the solution [10]. For the case above, a scaling factor can be calculated as

$$\sigma = \left[\sum_{i=1}^{2N+1} \beta_i^2 \right]^{1/2} \Big/ F. \tag{13}$$

Equation (10) in scaled form then becomes

$$\Delta s^2 = (F - F^k)^2 + \sum_{i=1}^{2N+1} \left(\frac{\beta_i - \beta_i^k}{\sigma} \right)^2, \tag{14}$$

where β_i^k and F^k refer to the previously converged solution, and β_i and F refer to the latest estimate of the solution.

Utilizing the above-described combination of harmonic balance and continuation techniques, the solution of the equation of motion can be represented by the coefficients of the Fourier series of θ as a function of the applied load, F, and forcing frequency, ω. In analyzing the fundamental response trajectories, ten coefficients ($C_0, C_1, \ldots, C_{10}$) and the associated phase angles ($\psi_0, \psi_1, \ldots, \psi_{10}$) were included in the solution process. Similarly, for the construction of subharmonic solution trajectories, the same ten coefficients and phase angles representig the fundamental response were included, along with the intermediate coefficients ($C_{1/2}, C_{3/2}, \ldots, C_{19/20}$) and phase angles ($\psi_{1/2}, \psi_{3/2}, \ldots, \psi_{19/20}$) representing the subharmonics. Typically, only the first three or four coefficients are required to characterize the solution.

The above techniques yield both stable and unstable solution branches; therefore, it is desirable to determine the stability of the periodic solutions found. The stability of the solutions is determined through the application of Floquet theory [11]. The general form of the equation of motion (3) can be written in first order form as

$$\dot{z}_1 = \dot{x}, \qquad \dot{z}_2 = \ddot{z}_1 = f(\dot{x}, x, t). \tag{15}$$

Linearizing equation (15) about the periodic solution $x_{mT}(t)$ gives

$$\dot{\mathbf{y}} = \mathbf{A(t)y}, \tag{16}$$

where

$$\mathbf{y} = \begin{Bmatrix} z_1 \\ z_2 \end{Bmatrix}, \tag{17}$$

and the terms of **A(t)** are defined as

$$A_{ij} = [\partial \dot{z}_i / \partial \dot{z}_j]_{x(t) = x_{mT}(t)}. \tag{18}$$

Thus, it is seen that **A(t)** is an mT-periodic matrix in time.

The solution of equation (17) after n periods of time can be written as

$$\mathbf{y}|_{t=nmT} = \mathbf{M}^n \mathbf{y}_0, \tag{19}$$

where $\mathbf{M}$ is the monodromy matrix [12]. The monodromy matrix is constructed by solving equation (17) using initial conditions of $\mathbf{y} = [1, 0]^T$ and $\mathbf{y} = [0, 1]^T$, resulting in the state vectors $\hat{\mathbf{y}}^1_{mT}$ and $\hat{\mathbf{y}}^2_{mT}$. Thus, the monodromy matrix is expressed as

$$\mathbf{M} = [\hat{\mathbf{y}}^1_{mT} \quad \hat{\mathbf{y}}^2_{mT}]. \tag{20}$$

Stability is easily ascertained for a given periodic solution using the eigenvalues, or Floquet multipliers, of the monodromy matrix. Since the Floquet multiplers may be complex quantities, their values are represented by a point in the real–imaginary plane. When the Floquet multipliers for a given periodic solution fall inside the unit circle, the periodic motion is stable. The opposite is true for periodic solutions resulting in Floquet multipliers with magnitudes larger than one. The Floquet multipliers also aid in identification of the various bifurcation points found in the solution space. As the stability along a given solution path is examined, the value of the Floquet multipliers will pass in and out of the unit circle along the real axis. Thus, any change in stability along a solution path occurs when the system parameters are such that the periodic solutions result in Floquet multipliers with values of ± 1. For the case of the periodic solutions producing Floquet multipliers with a value of 1, there exists a bifurcation and resulting change in stability. The particular type of bifurcation is dependent on the non-linear terms in the equation of motion. A passage of the Floquet multipliers through -1 indicates the existence of a period-doubling bifurcation, where the stable period one (1T) solution branch becomes unstable, and a new, stable period two (2T) solution branch emerges. Guckenheimer and Holmes [13] provide a detailed discussion of stability theory.

3. RESULTS

Utilizing the above-described combination of harmonic balance and continuation techniques, the solution of the equation of motion can be represented by plotting the coefficients of the Fourier series of $x(t)$ as a function of the applied load, F. The stable results were verified using numerical integration. In Figure 2 are shown the zero-, quarter-, half- and first order coefficients of the Fourier series as a function of the applied load. Selected details for the first order coefficient are shown in Figure 3. The solid lines represent solution trajectories determined to be stable by the Floquet analysis, and the dashed lines represent solution trajectories determined to be unstable by the Floquet analysis. Although other harmonics contribute to the solution of the equation of motion, the ones shown are sufficient to describe the qualitative characteristics of the solution. In all cases, harmonics up through C_5 were carried in the solution. In Figure 4 are shown phase-plane plots for various locations along the solution trajectories shown in Figure 2.

In interpreting the results shown in Figures 2 and 3, it is noted that for small values of the applied load F, two solutions exist, one stable, and one unstable. The stable solution corresponds to C_0 being non-zero. Two stable solutions exist, one about each of the stable static equilibrium positions. The particular response would be dependent on the initial conditions imparted to the system. This motion is asymmetric in the x–$\dot{x}$ phase plane. For the case of C_0 being equal to zero, the motion is a symmetric, unstable limit cycle about the unstable equilibrium position of $x = 0$. The symmetric solution branch exists for the entire range of the applied loading. These types of responses are those expected according to the theoretical and experimental work by Moon and Holmes [2], and coincide both

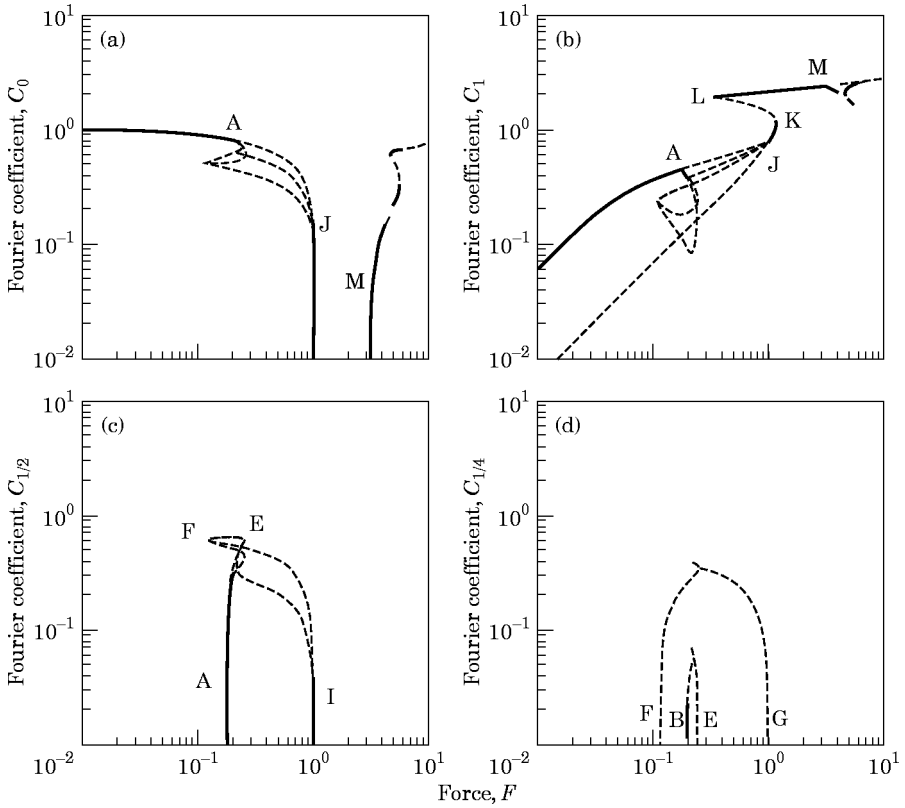

Figure 2. Selected Fourier coefficients for the periodic sloution to Duffing's equation. (a) The zero-order (mean value) component, C_0; (b) the fundamental component, C_1; (c) the half-order (2T-period) component, $C_{1/2}$; (d) the quarter-order (4T-period) component $C_{1/4}$. ——, Stable: – – –, unstable.

qualitatively and quantitatively with the results of Dowell and Pezeshki [4, 5, 8] described above.

The first bifurcation in the asymmetric solution branch occurs at $F = 0{\cdot}176$, point A in Figures 2 and 3(a). A change in stability is signified by one of the Floquet multipliers passing out of the unit circle along the neative real axis. Thus, a period-doubling bifurcation is encountered, and a period two, 2T, solution is born. This coincides with the Fourier coefficient $C_{1/2}$ becoming non-zero, as shown in Figure 2. The 2T solution path can easily be followed in Figure 3(a). At point B, another period-doubling bifurcation is encountered. The 2T solution branch experiences a loss of stability, and a stable, 4T solution is born and the Fourier coefficient $C_{1/4}$ becomes non-zero (Figure 2). At a slightly larger increase in the applied load, the 4T solution encounters a period-doubling bifurcation. Although it is not traced, an 8T solution would be born at this point. Thus, a period-doubling sequence has been initiated that would eventually lead to chaotic motion at a value in the neighborhood of $F = 0{\cdot}205$.

Continuing along the 4T path to point C, another period-doubling bifurcation point is encountered. At this point, the period-doubling sequence which began at point B will have reversed itself and the 8T branch will rejoin the 4T branch. At the horizontal asymptote of the 4T branch at point C, the branch regains stability. As the solution branch continues beyond point C, a change in stability is again encountered. Here, the Floquet multipliers pass out of the unit circle along the positive real axis, indicating a change in the

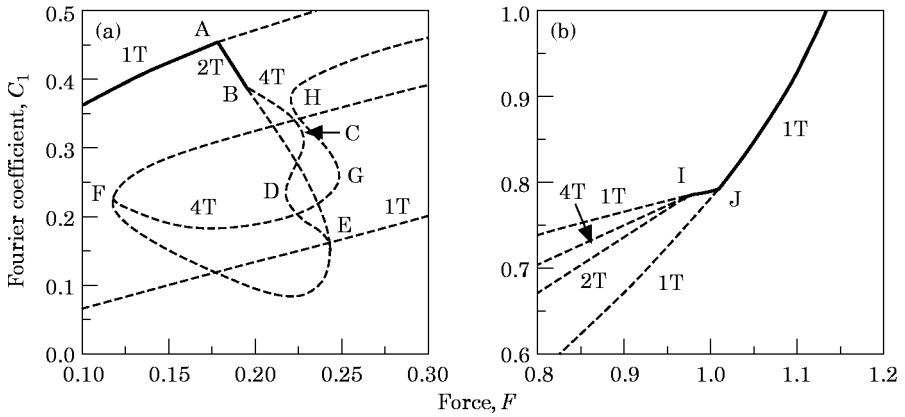

Figure 3. Selected details for the first order coefficinet, C_1, of Figure 2: ——, Stable; – – –, unstable.

configuration of the equilibrium solution. This can be evidenced by the phase-plane plots in Figure 4.

At point D, another period-doubling cascade initiates as the 4T branch passes through another region of stability at the horizontal asymptote. The period-doubling cascade reverses itself, and rejoins the 4T branch at point E. At the horizontal asymptote of the 2T branch at point E, the 4T branch rejoins the 2T branch. This corresponds to the $C_{1/4}$ coefficient going to zero, as seen in Figure 2. The 2T branch passes through a short range of stability, then loses stability at a symmetry-breaking bifurcation. At point F, the 2T solution again passes through a short region of stability. A period-doubling bifurcation

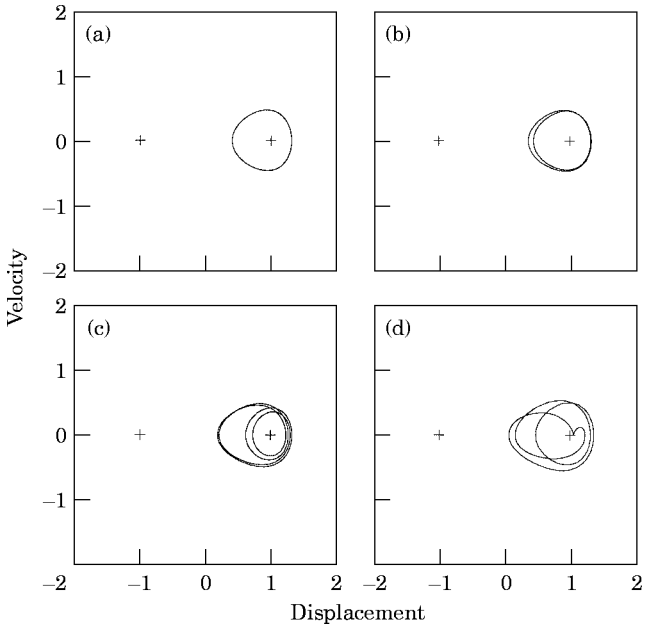

Figure 4. Phase-plane diagrams for selected values of the applied load. The period of response and locations refer to the solution trajectories presented in Figures 2 and 3: (a) $F = 0{\cdot}177$, 1T, location A; (b) $F = 0{\cdot}178$, 2T location B; (c) $F = 0{\cdot}197$, 4T, location C; (d) $F = 0{\cdot}228323$, 4T, location C; (e) $F = 0{\cdot}2177$, 4T, location D; (f) $F = 0{\cdot}2424$, 4T, location E; (g) $F = 0{\cdot}243$, 2T, location E; (h) $F = 0{\cdot}11646$, 2T, location F; (i) $F = 0{\cdot}1165$, 4T, location F; (j) $F = 0{\cdot}0{\cdot}21$, chaotic; (k) $F = 0{\cdot}24847$, 4T, location G; (l) $F = 0{\cdot}9668$, 4T, location I; (m) $F = 0{\cdot}97$, 2T, location I; (n) $F = 0{\cdot}99$, 1T, location J; (o) $F = 1{\cdot}15$, 1T, location K; (p) $F = 2{\cdot}0$, 1T, location M.

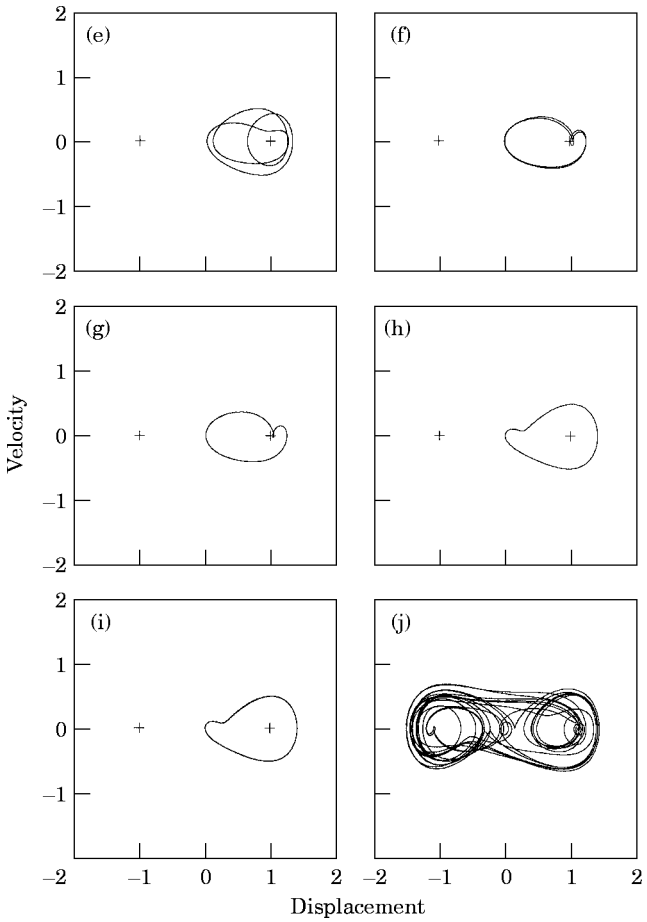

Figure 4—*continued*.

is encountered, and a new 4T solution emerges. This is evidenced by the re-emergence of the $C_{1/4}$ coefficient (Figure 2). The 4T solution loses stability immediately, and a period-doubling sequence leading to chaotic motion occurs again (Figure 4(j)). This sequence rejoins the 4T branch at point G, where the 4T branch passes through stability and another symmetry-breaking bifurcation. Another change in stability occurs at point H, where the 4T branch passes through a short region of stability, and then passes through another period-doubling cascade. This cascade reverses itself and rejoins the 4T solution branch at point I, as shown in Figure 3(b). The 4T solution branch and 2T solution branch are rejoined, and meet up with the asymmetric branch at point I. Note that the $C_{1/2}$ and $C_{1/4}$ coefficients both go to zero in this region (Figure 2).

At point J in Figure 2, the symmetric and asymmetric period-one branches join for the first time at a symmetry-breaking bifurcation, where stability passes from the asymmetric solution (Figure 4(a)) to the symmetric solution (Figure 4(o)). The loss of the asymmetric solution corresponds to the value of the C_0 coefficient going to zero. Note that the motion now encompasses all three equilibrium positions. At point K, a bifurcation point is again encountered corresponding to a change in the stability configuration of the system. Stability is regained at point L, at which the phase portrait now coincides with the typical large amplitude response about all three equilibrium positions. At point M, a symmetry-breaking bifurcation is encountered, and an asymmetric branch arises. C_0 is

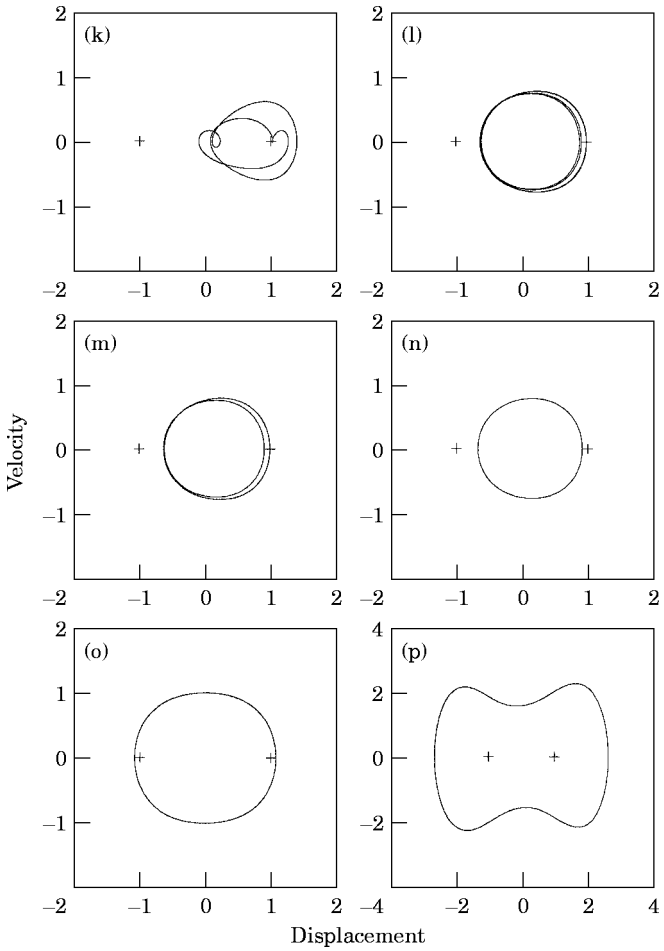

Figure 4—*continued*.

again non-zero. This asymmetric branch passes through period-doubling bifurcations and turning points. It is likely that some of these period-doubling bifurcations lead to period-doubling cascades and chaotic motion. None of these solution paths were pursued in this study. The characteristics of the solution paths described above are summarized in Table 1.

TABLE 1

Solution branch descriptions

Branch	Period	Stability	Branch	Period	Stability
A–B	2T	$<\pm 1$	G–H	4T	>1
B–C	4T	<-1	H–I	4T	<-1
C–D	4T	>1	I–J	2T	$<\pm 1$
D–E	4T	<-1	J–K	1T	$<\pm 1$
E–F	2T	>1	K–L	1T	>1
F–G	4T	<-1	L–M	1T	$<\pm 1$

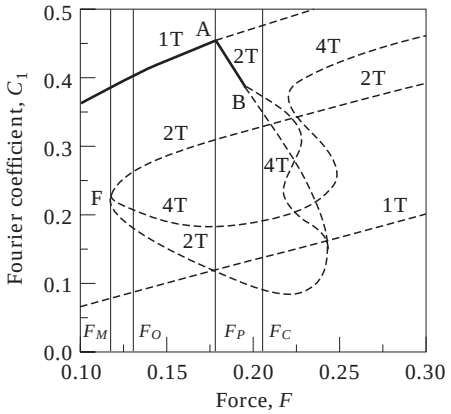

Figure 5. A comparison of results of previous research with those of the current study. F_M = Mel'nikov force value; F_O = observable chaos boundary; F_P = nominal period-doubling force; F_C = nominal chaos force. ——, Stable; – – –, unstable.

4. DISCUSSION

In comparing the results presented above with those of previous researchers, it is seen that all of the dynamic responses reported in the earlier work have been represented in this study as well. Both the stable periodic orbits about each of the static equilibrium positions for low levels of applied loading, as well as the large amplitude response motion about all three equilibrium positions, have been replicated. Additionally, all of the period-doubling and chaotic responses reported by other researchers have been observed, as shown in Figure 5. Since the harmonic balance technique allows for the discovery of unstable as well as stable solutions, several new features of the dynamic response are observed.

The nominal period-doubling force, $F_P = 0{\cdot}177$, identified by Pezeshki and Dowell [5] coincides with the first period-doubling bifurcation on the stable 1T solution branch at point A in Figure 5. However, this is not the minimum load value for which a stable 2T solution exists. As the 2T branch is traced, it is found to pass through a stable section at $F = 0{\cdot}1165$, point F in Figure 5. The branch in this region is stable for a very small range of the applied loading. The small range for which this 2T solution branch is stable would make it very difficult to detect this solution with the use of numerical integration techniques.

The results presented above allow for insight into the regions of applied loading in which one would expect to find chaotic response. Following along a given solution path until a period-doubling bifurcation occurs identifies a possible route to chaotic behavior. Identification of all of the period-doubling bifurcation points along a given route aids in determining where the period-doubled solutions begin and end. By then inspecting the 2T solution branches for period-doubling bifurcations, and tracing the resulting 4T solution paths, a complete picture of the ranges of applied loading likely to lead to chaotic response is developed. Higher period-doubled solutions could be traced using the same technique. However, the process becomes computationally expensive due to the large number of Fourier coefficients that must be carried in the solution process. Additionally, the load range over which the higher period solutions remain stable will continue to decrease, making it quite difficult to find the period-doubling bifurcations on the next higher solution branches. Thus, it is felt that the loss of stability at a period-doubling bifurcation of a 4T solution branch indicates the possibility of the location of a period-doubling cascade.

The lowest value of the applied load at which only chaotic response was observed by Dowell and Pezeshki [4] was reported as $F_C = 0{\cdot}205$. Indeed, this value corresponds to the first range of the applied load at which no stable periodic solution was found. Additionally, there is a 4T branch that goes through a period-doubling bifurcation at a load level just below $F = 0{\cdot}205$, point B in Figure 5. Viewing the stability characteristics of the other 4T solution branches in that range of applied load, it is evident that each of them have passed through a period-doubling bifurcation. Thus, a strange attractor exists for this range of applied loading. This phenomenon would be expected to be observable for load amplitudes up to the range of $F = 0{\cdot}97$, where the period-doubling cascade is observed to reverse itself, and superharmonic stable solutions are once again observed.

Since certain sets of initial conditions resulted in the observance of chaotic motion for $F_O = 0{\cdot}13$, Pezeshki and Dowell [5] had hypothesized the existence of a strange attractor for that range of the applied load. This would coincide with the period-doubling sequence initiating from the 2T solution branch at point F in Figure 5. That particular 4T solution branch remains unstable over the range of $0{\cdot}1165 < F < 0{\cdot}24$. Should a basin boundary map be developed for this load range, it would be expected that the domain of attraction of the chaotic solution would be quite small.

Finally, the load value for which the stable and unstable manifolds intersected was predicted by the Mel'nikov criterion to be $F_M = 0{\cdot}1176$. Based on the results shown above, this appears to be a very accurate indicator of the onset of an interesting dynamic response. This value of the applied load corresponds very closely to the minimum load value at which a period-doubling route to chaos is observed. Additionally, the existence of the stable superharmonic solutions at that load range explain the fractal behavior observed in the basin boundary maps around the Mel'nikov force level. Since there are in fact more than two stable, 1T limit cycle responses for this load range, the fractal behavior of the basin boundary maps would be expected.

The dynamic buckling response is also easily observed using this type of analysis. Although no range of the applied loading showed coexisting regions of stable amplitude response about one equilibrium position and stable large amplitude response about all the equilibrium positions, it is evident that the range over which neither of these solutions are stable is quite small. Additionally, there is a short range of applied loading over which there are two stable, symmetric large amplitude responses.

5. CONCLUSIONS

The harmonic balance technique coupled with the continuation scheme was able to track the various branches of the solution to Duffing's equation. With the use of Floquet analysis, the stability characteristics of each of the branches were determined. Thus, a complete picture of the solution trajectories for a range of applied loading was determined. The importance of tracing the unstable solution trajectories was demonstrated by finding previously undetected stable periodic and superharmonic solutions, as well as strange attractors arising from period-doubling bifurcation points along these trajectories.

As predicted, the discrepancies between the predicted and observed load values for the onset of chaotic response and the fractal behavior of the basin boundary maps is shown to be the result of coexisting solution trajectories. For different ranges of the applied loading, basins of attraction were found to simultaneously exist for periodic 1T responses and superharmonic responses, for periodic 1T responses and chaotic responses, and for pairs of periodic 1T responses. The existence of these basins of attraction are independent of the initial conditions imparted to the system.

In conclusion, the utilization of the harmonic balance technique coupled with a continuation scheme and subsequent stability analysis is shown to be a very viable method to use for the detection of superharmonic responses as well as chaotic attractors.

REFERENCES

1. P. Holmes 1979 *Philosophical Transactions of the Royal Society of London* **294**, 419–448. A nonlinear oscillator with a strange attractor.
2. F. C. Moon and P. J. Holmes 1979 *Journal of Sound and Vibration* **65**, 275–296. A magnetoelastic strange attractor.
3. V. K. Mel'nikov 1963 *Transactions of the Moscow Mathematical Society* **12**, 1–57. On the stability of the center for time periodic perturbations.
4. E. H. Dowell and C. Pezeshki 1986 *Journal of Applied Mechanics* **53**, 5–9. On the understanding of chaos in Duffing's equation including a comparison with experiment.
5. C. Pezeshki and E. H. Dowell 1987 *Journal of Sound and Vibration* **117**, 219–232. An examination of initial condition maps for the sinusoidally excited buckled beam modeled by the Duffing's equation.
6. F. C. Moon 1980 *Journal of Applied Mechanics* **47**, 638–644. Experiments of chaotic motions of a forced nonlinear oscillator: strange attractors.
7. P. J. Holmes and F. C. Moon 1983 *Journal of Applied Mechanics* **50**, 1021–1032. Strange attractors and chaos in nonlinear mechanics.
8. E. H. Dowell and C. Pezeshki 1988 *Journal of Sound and Vibration* **121**, 195–200. On necessary and sufficient conditions for chaos to occur in Duffing's equation: an heuristic approach.
9. A. Y. T. Leung and T. C. Fung 1989 *International Journal of Numerical Methods in Engineering* **28**, 193–209. Phase increment analysis of damped Duffing oscillators.
10. R. Seydel 1988 *From Equilibrium to Chaos*. New York: Elsevier.
11. J. M. T. Thompson and H. B. Stewart 1986 *Nonlinear Dynamics and Chaos*. New York: John Wiley.
12. D. W. Jordon and P. Smith 1977 *Nonlinear Differential Equations*. Oxford: Clarendon Press.
13. J. Guckehneimer and P. Holmes 1983 *Nonlinear Oscillations*, *Dynamical Systems*, *and Bifurcations of Vector Fields*. New York: Springer-Verlag.